

# New determination of structure parameters in strong field tunneling ionization theory of molecules

Song-Feng Zhao,<sup>1,2</sup> Cheng Jin,<sup>1,2</sup> Anh-Thu Le,<sup>1</sup> T. F. Jiang,<sup>1,3</sup> and C. D. Lin<sup>1</sup>

<sup>1</sup>*J. R. Macdonald Laboratory, Physics Department,*

*Kansas State University, Manhattan, Kansas 66506-2604, USA*

<sup>2</sup>*College of Physics and Electronic Engineering, Northwest Normal University,*  
*Lanzhou, Gansu 730070, People's Republic of China*

<sup>3</sup>*Institute of Physics, National Chiao-Tung University, Hsinchu 30010 Taiwan*

(Dated: May 31, 2018)

In the strong field molecular tunneling ionization theory of Tong *et al.* [Phys. Rev. A **66**, 033402 (2002)], the ionization rate depends on the asymptotic wavefunction of the molecular orbital from which the electron is removed. The orbital wavefunctions obtained from standard quantum chemistry packages in general are not good enough in the asymptotic region. Here we construct a one-electron model potential for several linear molecules using density functional theory (DFT). We show that the asymptotic wavefunction can be improved with an iteration method and after one iteration accurate asymptotic wavefunctions and structure parameters are determined. With the new parameters we examine the alignment-dependent tunneling ionization probabilities for several molecules and compare with other calculations and with recent measurements, including ionization from inner molecular orbitals.

PACS numbers: 33.80.Rv, 42.50.Hz

## I. INTRODUCTION

Tunneling ionization of molecules in strong infrared fields is the first step in many interesting strong-field phenomena such as high-order harmonic generation (HHG), emission of high-energy above-threshold ionization (HATI) electrons and non-sequential double ionization (NSDI). Essential understanding to these processes is the angle-dependent ionization probability  $P(\theta)$  for a molecule fixed in space, where  $\theta$  is the angle between the molecular axis and the polarization direction of the laser's electric field. Since molecules are generally not fixed in space, i.e., not at a fixed alignment and/or orientation, experimental determination of  $P(\theta)$  from partially aligned molecules requires additional assumptions. Alnaser *et al.* [1] first determined  $P(\theta)$  from NSDI processes where the alignment of the molecule is determined by Coulomb explosion of the molecular ions.  $P(\theta)$  can also be determined by ionizing partially aligned molecules [2, 3], or by measuring the angular distribution of electrons removed by a circularly polarized laser [4, 5]. In both methods the alignment of the molecular axis is determined by Coulomb explosion when the molecular ion is further ionized by an intense circularly polarized laser. In all of these measurements, the  $P(\theta)$  is not determined directly for a fixed angle and some approximations are used in order to determine the alignment-dependent ionization probability.

Theoretically,  $P(\theta)$  can in principle be obtained directly from numerical solution of the time-dependent Schrödinger equation (TDSE). However, even for the simplest  $H_2^+$ , the  $P(\theta)$  obtained from solving TDSE by different groups still exhibits relatively large differences. While calculations of  $P(\theta)$  for interesting multi-electron molecular systems have been carried out using

the time-dependent density-functional theory (TDDFT) (see, for example, [6]), the accuracy of these calculations is difficult to evaluate. Furthermore, these calculations are rather time-consuming. Beside these *ab initio* approaches, alignment-dependent tunneling ionization rate for molecules can be calculated using simple models such as the molecular strong field approximation (SFA) [7, 8], or the molecular tunneling ionization theory [9]. The latter is the simplest and is a generalization of the tunneling model of Ammosov, Delone and Krainov (ADK) [10] for atoms. In the molecular tunneling ionization model (MO-ADK) of Tong *et al.* [9], the ionization rate for a molecule aligned at an angle  $\theta$  with respect to the laser polarization axis is given analytically. The ionization rate depends on the instantaneous electric field of the laser, the ionization potential of the molecule and some structure parameters of the orbital wavefunction in the asymptotic region. Subsequent further extension of the MO-ADK theory can be found in [11–13].

In Tong *et al.* [9], the structure parameters are extracted from molecular wavefunctions calculated using the multiple scattering method [14]. However, these days molecular wavefunctions are more easily accessible from quantum chemistry packages such as GAMESS [15], GAUSSIAN [16] and others. Thus it is desirable to obtain structure parameters from the asymptotic behavior of orbitals calculated from such packages. This was carried out for  $CO_2$  by Le *et al.* [17] and for other molecules by Kjeldsen and Madsen [18]. Unfortunately, molecular orbitals from these chemistry packages are calculated using gaussian basis functions and they are not suitable for representing the exponential decay of the wavefunction at large distances. As more accurate experimental data are becoming available, it is essential to redetermine these structure parameters more accurately. Since

the asymptotic wavefunction does not contribute much to the total energy of a molecule, one cannot efficiently improve the asymptotic wavefunctions by enlarging the size of the gaussian basis directly.

In this paper, we describe how to improve the asymptotic wavefunction where the structure parameters are extracted. Our input consists of wavefunctions of all the occupied orbitals obtained from GAMESS or GAUSSIAN. We then construct a single-active-electron model potential and solve the time-independent Schrödinger equation to obtain the molecular orbital wavefunctions by an iterative procedure. The details of the method are given in Section II. We then apply the method to redetermine all the structure parameters previously published in [9], and adding structure parameters for some inner orbitals. We also determine the structure parameters for a number of systems that have been investigated experimentally. Using these new structure parameters we examined the alignment dependence of ionization probabilities for several systems. In most cases, the new results do not differ much from what were presented in Tong *et al.* [9]. However, there are differences in some molecules. The strong deviation in CO<sub>2</sub> has been reported recently [19].

## II. THEORETICAL METHODS

The theory part is divided into three subsections. We first present the method of generating a single-active-electron model potential for linear molecules. We then discuss how to calculate the wavefunctions by solving the time-independent Schrödinger equation with B-spline basis functions. We will also briefly describe how to extract the structure parameters in the MO-ADK theory.

### A. Construction of single-active-electron model potentials for linear molecules

Single-active-electron model potential approach has been widely used for describing atoms in strong-field physics (see, for example, [20]). This approach has also been used for molecular targets recently [19, 21]. The one-electron model potential consists of two parts: electrostatic and exchange-correlation terms. It is well-known that the traditional local-density approximation (LDA) for the exchange-correlation potential does not give the correct  $(-1/r)$  potential in the asymptotic region where the structure parameters are to be extracted. In this paper, we follow Abu-samha and Madsen [21] and use the LB potential, proposed by Leeuwen and Baerends [22], which will give the correct asymptotic  $-1/r$  behavior for neutral atoms and molecules. We note that a similar LB potential, called LB $\alpha$  [23], has also been used by Chu and collaborators in their TDDFT approach [6, 24].

For linear molecules, the model potential can be ex-

pressed in single-center expansion as

$$V(r, \theta) = \sum_{l=0}^{l_{max}} v_l(r) P_l(\cos \theta). \quad (1)$$

Here,  $v_l(r)$  is the radial component of the model potential and  $P_l(\cos \theta)$  the Legendre polynomial. Typically we choose  $l_{max} = 40$ . The radial potential is given by

$$v_l(r) = v_l^{nuc}(r) + v_l^{el}(r) + v_l^{ex}(r), \quad (2)$$

where the first two terms represent the electrostatic potential and the last term is the exchange interaction.

The electron-nucleus interaction  $v_l^{nuc}(r)$  can be written as

$$v_l^{nuc}(r) = \sum_{i=1}^{N_a} v_l^i(r), \quad (3)$$

where  $i$  runs over the  $N_a$  atoms in the molecule. Without loss of generality, we assume that linear molecules are aligned along the  $z$ -axis, then  $v_l^i(r)$  can be expressed as

$$v_l^i(r) = \begin{cases} -(\frac{r_{<}^i}{r_{>}^i})^l \frac{Z_c^i}{r_{>}^i} & \text{for } z_i > 0 \\ -(-1)^l (\frac{r_{<}^i}{r_{>}^i})^l \frac{Z_c^i}{r_{>}^i} & \text{for } z_i < 0 \end{cases} \quad (4)$$

with  $r_{<}^i = \min(r, |z_i|)$ ,  $r_{>}^i = \max(r, |z_i|)$ . Here  $Z_c^i$  and  $z_i$  are the nuclear charge and the  $z$  coordinate of the  $i$ th atom, respectively.

The partial Hartree potential  $v_l^{el}(r)$  is given by

$$v_l^{el}(r) = \frac{4\pi}{2l+1} \int_0^\infty a_l(r') r'^2 \frac{r_{<}^l}{r_{>}^{l+1}} dr' \quad (5)$$

with  $r_{<} = \min(r, r')$ ,  $r_{>} = \max(r, r')$ . Here  $a_l(r')$  is

$$a_l(r') = \frac{2l+1}{2} \int_{-1}^1 \rho(r', \theta') P_l(\cos \theta') d(\cos \theta'), \quad (6)$$

where  $\rho$  is the total electron density in the molecule and

$$\rho(r', \theta') = \sum_{i=1}^{N_e} \frac{1}{2\pi} \int_0^{2\pi} |\Psi_i(r', \theta', \varphi')|^2 d\varphi'. \quad (7)$$

Here  $i$  runs over all the  $N_e$  electrons in the molecule. The wavefunction of each molecular orbital can be obtained from quantum chemistry packages such as GAMESS [15] or GAUSSIAN [16].

For the partial exchange potential, it is written as

$$v_l^{ex}(r) = \frac{2l+1}{2} \int_{-1}^1 V_{ex,\sigma}(r, \theta) P_l(\cos \theta) d(\cos \theta), \quad (8)$$

where

$$V_{ex,\sigma}(r, \theta) = \alpha V_{ex,\sigma}^{LDA}(r, \theta) + V_{ex,\sigma}^{GC}(r, \theta) \quad (9)$$

Here  $V_{ex,\sigma}^{LDA}(r, \theta)$  is the LDA potential for an electron with spin  $\sigma$

$$V_{ex,\sigma}^{LDA}(r, \theta) = -\left[\frac{6}{\pi}\rho_\sigma(r, \theta)\right]^{1/3}, \quad (10)$$

where

$$\rho_\sigma(r, \theta) = \sum_{i=1}^{N_\sigma} \frac{1}{2\pi} \int_0^{2\pi} |\Psi_{i\sigma}(r, \theta, \varphi)|^2 d\varphi. \quad (11)$$

Here  $i$  runs over the  $N_\sigma$  electrons that have the same spin as the active electron. The gradient correction term is given by [22]

$$V_{ex,\sigma}^{GC}(r, \theta) = -\frac{\beta\chi_\sigma^2(r, \theta)\rho_\sigma^{1/3}(r, \theta)}{1 + 3\beta\chi_\sigma(r, \theta)\sinh^{-1}(\chi_\sigma(r, \theta))}, \quad (12)$$

where  $\chi_\sigma(r, \theta) = |\nabla\rho_\sigma(r, \theta)|\rho_\sigma^{-4/3}(r, \theta)$ . The parameters  $\alpha$  and  $\beta$  are chosen to be 1.0 and 0.05, respectively throughout this paper. We note that for more accurate binding energies, the correlation potential should be included into Eq. (9). In the so-called LB $\alpha$  model, the two parameters  $\alpha$  and  $\beta$  are usually chosen to be 1.19 and 0.01, respectively (see, [23]).

### B. Calculation of molecular wavefunctions by solving the time-independent Schrödinger equation

With the model potential constructed in the previous subsection, the wavefunction for the active electron in a linear molecule can be obtained by solving the following time-independent Schrödinger equation

$$H_{el}\psi_n^{(m)}(\mathbf{r}) \equiv \left[-\frac{1}{2}\nabla^2 + V(r, \theta)\right]\psi_n^{(m)}(\mathbf{r}) = E_n\psi_n^{(m)}(\mathbf{r}) \quad (13)$$

where  $\psi_n^{(m)}$  and  $E_n^{(m)}$  are the eigenfunction and eigenvalue, respectively.

Using single-center expansion for the electronic wavefunction

$$\psi_n^{(m)}(\mathbf{r}) = \sum_{l=0}^{l_{max}} \frac{u_{nl}(r)}{r} Y_{lm}(\theta, \varphi) \quad (14)$$

where  $Y_{lm}(\theta, \varphi)$  are the spherical harmonics, the radial wavefunction can be constructed with B-splines [25]

$$u_{nl}(r) = \sum_{i=1}^{N_l} c_{il}^n B_i(r). \quad (15)$$

Substituting Eqs. (1), (14) and (15) into Eq. (13) and then projecting onto the  $B_i Y_{lm}^*$  basis, we obtain the following matrix equation

$$HC = ESC \quad (16)$$

where

$$H_{il,i'l'} = \frac{\int_0^{r_{max}} \int_0^\pi \int_0^{2\pi} B_i(r) Y_{lm}^*(\theta, \varphi) H_{el} B_{i'} Y_{l'm'}(\theta, \varphi) dr \sin\theta d\theta d\varphi}{B_{i'} Y_{l'm'}(\theta, \varphi)} \quad (17)$$

$$S_{il,i'l'} = \delta_{ll'} \int_0^{r_{max}} B_i(r) B_{i'}(r) dr \quad (18)$$

The eigenfunctions and eigenvalues are obtained by diagonalizing Eq. (16).

### C. Extracting asymptotic structure parameters

In the asymptotic region, typically only a few terms in the single-center expansion Eq. (14) are important. Following Tong *et al.* [9], we write the wavefunction of a linear molecule as

$$\psi_n^{(m)}(\mathbf{r}) = \sum_l F_{lm}(r) Y_{lm}(\theta, \varphi). \quad (19)$$

In the MO-ADK theory [9], the radial functions in the asymptotic region are fitted to the following form

$$F_{lm}(r) = C_{lm} r^{(Z_c/\kappa)-1} e^{-\kappa r} \quad (20)$$

where  $Z_c$  is the asymptotic charge,  $\kappa = \sqrt{2I_p}$ ,  $I_p$  is the ionization energy.

## III. RESULTS AND DISCUSSION

### A. On the quality of the model potential and the iteration procedure

In this paper, the single-active-electron model potential [see Sec. II A] is created with the DFT, in which the exchange potential is constructed with the exchange-only LDA potential and the LB model potential (or LDA+LB). First we check the quality of this model potential if the molecular orbitals obtained from the standard quantum chemistry package GAMESS [15] are used as the input.

In Fig. 1(a), we compare the present  $r$ -weighted LB potential with the empirical model potential of Tong *et al.* [20] for Ne. For clarity we plot the effective charge, defined as  $r \times V(r)$ . The two potentials agree well in the small  $r$  region. However, there are significant differences at large  $r$ . For neutral atoms, the effective charge should approach -1 at large  $r$ . If the LB potential is calculated directly using the molecular wavefunctions from GAMESS (dashed line) the effective charge exhibits oscillations and then drops rapidly with  $r$ . This undesirable behavior is due to the incorrect electron density, which in turn is due to the limitation of the gaussian basis, calculated from GAMESS in the large  $r$  region.

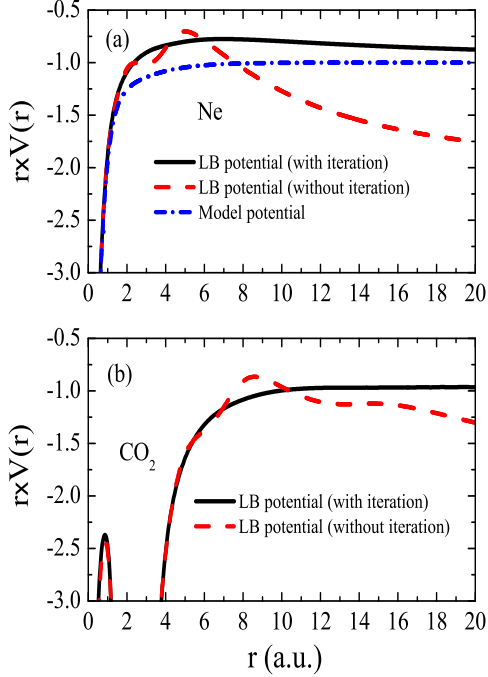


FIG. 1: (Color online) (a) Effective charge of Ne with and without the iteration (see text). Model potential is from [20]. (b) Effective charge of  $CO_2$  along the molecular axis.

To correct this error, we perform one more iteration on the potential: Firstly, an initial model potential is generated using the Hartree-Fock (HF) wavefunctions obtained from GAMESS. From this initial potential, more accurate wavefunctions are obtained by solving Eq. (13) with B-spline basis. Then, a new model potential is constructed from these new wavefunctions. From Fig. 1(a), we observe that the effective charge obtained after one iteration (solid line) shows the correct asymptotic behavior. The same procedure can be applied to molecules. In Fig. 1(b), we show the model potential of  $CO_2$  along the molecular axis, with and without one iteration. It confirms that the asymptotic behavior of the model potential is correct after one iteration. We comment that in the case of  $CO_2$  diffuse functions have been included in the basis sets. Clearly, this alone is insufficient for obtaining accurate electron density (or potential) at large  $r$ .

### B. Extracting molecular structure parameters for the MO-ADK theory

Once the model potential is obtained, the eigenfunction and eigenvalue can be calculated from solving Eq. (13). In Table I, binding energies of rare gas atoms obtained using the present method are compared to those from Ref. [26] and the experimental values. Our

TABLE I: Comparison of calculated ionization energies of rare gas atoms in the exchange-only LDA+LB model and experimental values.

Atom	LDA+LB (a.u.)	$I_p$ (a.u.)
He	0.786	0.904 <sup>a</sup>
	0.796 <sup>b</sup>	
Ne	0.722	0.793 <sup>a</sup>
	0.725 <sup>b</sup>	
Ar	0.524	0.579 <sup>a</sup>
	0.528 <sup>b</sup>	
Kr	0.499	0.515 <sup>a</sup>
Xe	0.469	0.446 <sup>a</sup>

<sup>a</sup>Reference[27]

<sup>b</sup>Reference[26]

TABLE II: Equilibrium distances, ionization energies calculated in the exchange-only LDA+LB model, and experimental vertical ionization potentials for several linear molecules.

Molecule	R (Å)	LDA+LB (eV)	$I_p$ (eV)
$H_2^+$	1.058	29.99	29.99
$D_2$	0.742	13.65	15.47
$N_2$	1.098	14.99	15.58
$O_2$	1.208	10.62	12.03
$F_2$	1.412	16.03	15.70
$S_2$	1.889	10.36	9.36
CO	1.128	13.22	14.01
NO	1.151	9.14	9.26
SO	1.481	9.37	10.29
$CO_2$	1.163	14.63	13.78
$C_2H_2$	1.203 ( $R_{CC}$ )	11.19	11.41
	1.058 ( $R_{CH}$ )		
HF	0.917	15.03	15.77
HCl	1.275	11.41	12.75
HCN	1.067 ( $R_{CH}$ )	13.46	13.80
	1.159 ( $R_{CN}$ )		

method uses the same approximate exchange potential as in Ref. [26]. The two calculations agree in general, but small discrepancies do exist with experimental values. These discrepancies can be reduced if correlation potential is included in Eq. (9). This fact has been well documented in Ref. [26].

In Table II, we compare the ionization energies from the present calculations with experimental vertical ionization energies for several linear molecules. The equilibrium distances of these molecules are also listed. The agreement between the calculated and experimental values are good. Again we comment that the exchange-only LDA+LB potential are used in our calculations. For higher precision, correlation potential should be included [6, 23, 24, 28].

TABLE III: The newly fitted  $C_{lm}$  coefficients vs values from earlier references, [9, 17, 29, 30].

Molecule	$C_{0m}$	$C_{1m}$	$C_{2m}$	$C_{3m}$	$C_{4m}$	$C_{5m}$	$C_{6m}$
$H_2^+(\sigma_g)$	4.52		0.62		0.03		
	4.37		0.05		0.00		[9]
$D_2(\sigma_g)$	1.78		0.11		0.00		
	2.51		0.06		0.00		[9]
	1.15		0.067		0.001		[29]
$N_2(\sigma_g)$	2.68		1.10		0.06		
	2.02		0.78		0.04		[9]
$O_2(\pi_g)$			0.52		0.03		
			0.62		0.03		[9]
$F_2(\pi_g)$			1.21		0.13		
			1.17		0.13		[9]
$S_2(\pi_g)$			1.37		0.17		
			0.81		0.07		[9]
$CO(\sigma)$	2.32	1.62	0.82	0.17	0.05		
	1.43	0.76	0.28	0.02	0.00		[9]
$NO(\pi)$		0.21	0.38	0.02	0.02		
		0.22	0.41	0.01	0.00		[9]
$SO(\pi)$		0.38	0.71	0.05	0.05		
		0.41	-0.31	0.01	0.00		[9]
$CO_2(\pi_g)$			1.97		0.40		0.04
			2.88		1.71		0.43 [17]
$C_2H_2(\pi_u)$		1.16		0.18		0.02	
		1.14		0.27		0.04	[30]
$HF(\pi)$		0.88	0.03	0.02	0.01		
$HCl(\pi)$		1.23	0.01	0.05	0.01	0.01	
$HCN(\pi)$		1.50	0.09	0.24	0.02	0.02	

With the new wavefunctions, we re-evaluate the structure parameters for a number of linear molecules. Table III lists the newly fitted  $C_{lm}$  coefficients with those listed in Tong *et al.* [9] and in others, if available. These parameters will be used to obtain the alignment-dependent tunneling ionization rates, following the MO-ADK theory [9].

### C. Comparison of alignment-dependent ionization probabilities between MO-ADK and other calculations

Using the improved structure parameters tabulated in Table III, we now use the analytical formula in Tong *et al.* [9] to obtain alignment-dependent tunneling ionization probabilities for selected molecules that have also been carried out by other methods. The results are shown in Fig. 2. For simplicity, all the probabilities are normalized to 1.0 at the peak. First, we comment that for  $N_2$ ,  $O_2$ ,  $F_2$  the normalized probabilities obtained using the new structure parameters do not show noticeable differences compared to the probabilities calculated using old struc-

ture parameters. From Table III, we note that the structure parameters for these three molecules do not change much. We emphasize that in calculating MO-ADK rates, one should always use the experimental vertical ionization energy since the tunneling ionization rate depends exponentially on the ionization potential. In Figs. 2(d) and 2(e), we notice that, interestingly, the MO-ADK results using the new  $C_{lm}$  give stronger angular dependence than the old ones for both  $H_2^+$  and  $H_2$ . This is the result of the relatively larger  $C_{2m}$  as compared to  $C_{0m}$  in the present calculations. For  $H_2^+$ , the present result lies between the two calculations from solving TDSE. For  $H_2$ , we compare the new results with those from SFA, and the two agree quite well. For  $C_2H_2$ , the new MO-ADK result agrees with the SFA, but differs from the older MO-ADK [30]. We comment that in the SFA calculation, wavefunctions directly from the GAMESS code are used. In general, SFA calculations yield incorrect total ionization rates. Empirically, however, the normalized alignment dependence from the SFA appears to be in agreement with the present MO-ADK. In presenting the SFA results, we always use the renormalized ones. We further comment that in SFA and other *ab initio* calculations, ionization probability or rate for each alignment angle is calculated independently. In the MO-ADK theory, the alignment dependence is obtained analytically after the structure parameters are obtained.

In recent years, *ab initio* calculations of molecular ionization by intense lasers have been carried out by solving the TDDFT [6, 28, 31]. These calculations include all the electrons in the molecule. Comparing to MO-ADK, in general, these calculations tend to give larger probabilities at angles where the ionization is small, see  $N_2$  near  $90^\circ$  and  $O_2$  and  $F_2$  at angles near  $0^\circ$  and  $90^\circ$ . For  $C_2H_2$ , on the other hand, the TDDFT result is smaller at smaller angles than the present one. For this system, it was carried out by a different group [31]. Based on these results we can say that the alignment dependence of the ionization probabilities obtained from MO-ADK and from TDDFT are in reasonable agreement. However, we mention that probabilities in Fig. 2 from MO-ADK include ionization from the HOMO only, while the many-electron TDDFT calculations show significant contributions from the inner orbitals. More on the comparison between MO-ADK and TDDFT will be given later.

### D. Alignment dependence of ionization rates from HOMO, HOMO-1 and HOMO-2 orbitals

Recently, strong field ionization phenomena involving inner orbitals of molecules have been reported widely [5, 34–37]. This is somewhat surprising since tunneling ionization rate decreases very rapidly with the increase of ionization potential. However, molecular tunneling ionization rates depend on the symmetry of the orbital wavefunctions. For alignment angles where  $P(\theta)$  is near the minimum for the HOMO but where HOMO-1

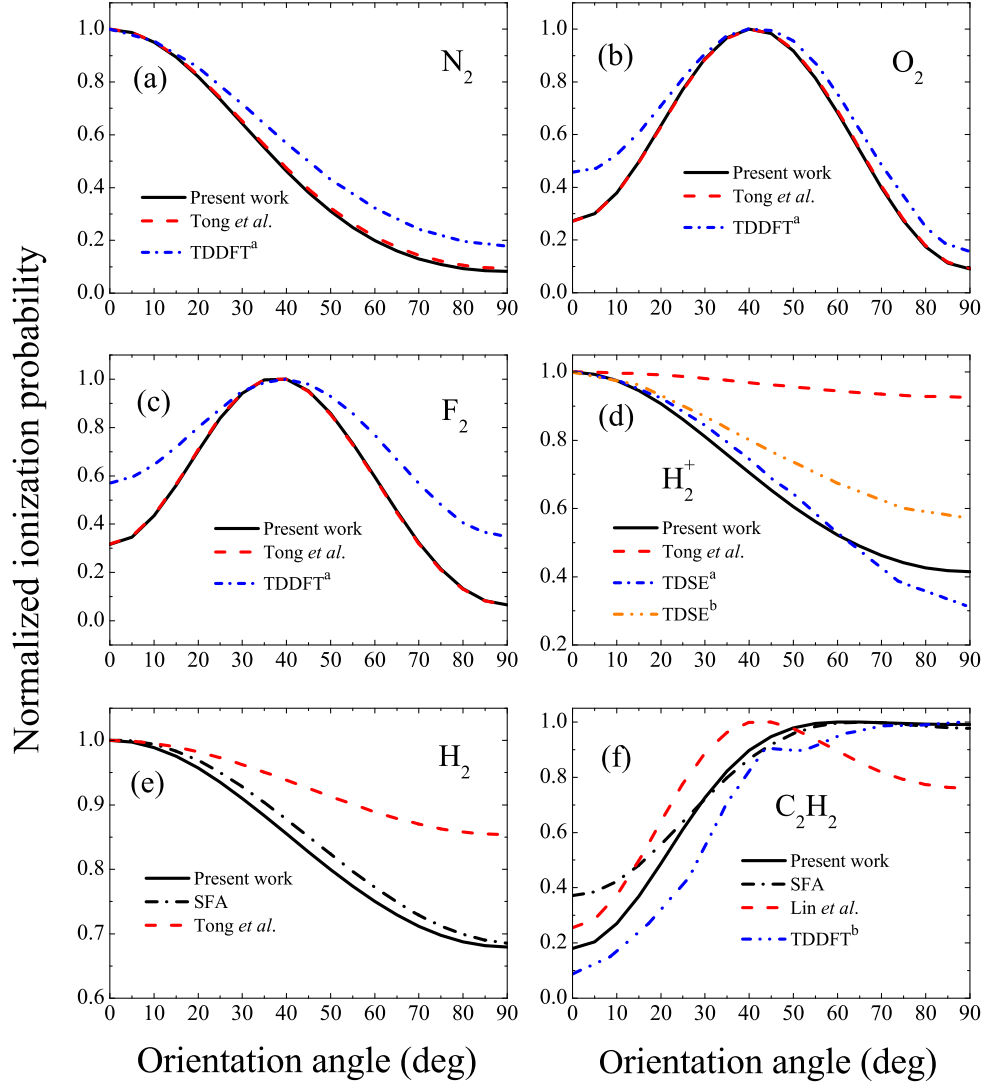


FIG. 2: (Color online) Normalized alignment dependence of ionization probability. (a)  $\text{N}_2$  at laser intensity of  $10^{14}$  W/cm<sup>2</sup>; (b)  $\text{O}_2$  at  $10^{14}$  W/cm<sup>2</sup>; (c)  $\text{F}_2$  at  $2 \times 10^{14}$  W/cm<sup>2</sup>; (d)  $\text{H}_2^+$  at  $5 \times 10^{14}$  W/cm<sup>2</sup>; (e)  $\text{H}_2$  at  $2.3 \times 10^{14}$  W/cm<sup>2</sup>; (f)  $\text{C}_2\text{H}_2$  at  $5 \times 10^{13}$  W/cm<sup>2</sup>. TDDFT<sup>a</sup> from Telnov *et al.* [28], TDDFT<sup>b</sup> from Otobe *et al.* [31], TDSE<sup>a</sup> from Kamta *et al.* [32], TDSE<sup>b</sup> from Kjeldsen *et al.* [33], Tong *et al.* from [9] and Lin *et al.* from [30].

is near the maximum, there is a good possibility that ionization from HOMO-1 can become comparable or higher than from HOMO. Indeed, contribution from HOMO-1 to high-order harmonic generation (HHG) from  $\text{N}_2$  molecules has been reported by McFarland *et al.* [34] when the molecules are aligned perpendicular to the polarization of the probe laser. Le *et al.* [35] have successfully reproduced the experimental results by including HHG from HOMO and HOMO-1. Since tunneling ionization is the first step for all rescattering processes [38–41], including HHG [40], it is pertinent to investigate

$P(\theta)$  from inner orbitals as well.

In Table IV, the binding energies of HOMO, HOMO-1 and HOMO-2 for several molecules are shown. These energies are compared to calculations using the  $\text{LB}\alpha$  model and experimental values, to check the relative accuracy of the model we have used. We emphasize again that accurate experimental ionization energies, not the theoretical values in the Table, are used in calculating the MO-ADK rates. The extracted  $C_{lm}$  parameters are given in Table V. Using these parameters and experimental ionization energies, the alignment dependence of ionization rates from different orbitals at a given peak laser intensity can

TABLE IV: Comparison of calculated binding energies of HOMO, HOMO-1 and HOMO-2 of N<sub>2</sub>, O<sub>2</sub> and CO<sub>2</sub> in the present exchange-only LDA+LB model. Those from the LB $\alpha$  model and experimental vertical ionization potential are also given. Energies are in electron volts. For CO, HCl and C<sub>2</sub>H<sub>2</sub>, only the energies of HOMO and HOMO-1 are considered.

Molecule	Spin orbital	LDA+LB	LB $\alpha$	I <sub>p</sub>
N <sub>2</sub>	3 $\sigma_g$ (HOMO)	15.0	15.5 <sup>a</sup>	15.6 <sup>b</sup>
	1 $\pi_u$ (HOMO-1)	16.5	16.9 <sup>a</sup>	17.2 <sup>b</sup>
	2 $\sigma_u$ (HOMO-2)	17.8	18.5 <sup>a</sup>	18.7 <sup>b</sup>
O <sub>2</sub>	1 $\pi_g$ (HOMO)	10.6	12.8 <sup>a</sup>	12.3 <sup>c</sup>
	1 $\pi_u$ (HOMO-1)	17.3	17.4 <sup>a</sup>	16.7 <sup>c</sup>
	3 $\sigma_g$ (HOMO-2)	17.1	18.3 <sup>a</sup>	18.2 <sup>c</sup>
CO <sub>2</sub>	1 $\pi_g$ (HOMO)	14.6	13.9 <sup>d</sup>	13.8 <sup>e</sup>
	1 $\pi_u$ (HOMO-1)	18.3	17.5 <sup>d</sup>	17.6 <sup>e</sup>
	3 $\sigma_u$ (HOMO-2)	16.8	17.2 <sup>d</sup>	18.1 <sup>e</sup>
CO	5 $\sigma$ (HOMO)	13.2		14.0 <sup>e</sup>
	1 $\pi$ (HOMO-1)	16.6		16.9 <sup>e</sup>
HCl	2 $\pi$ (HOMO)	11.4		12.8 <sup>f</sup>
	5 $\sigma$ (HOMO-1)	15.0		16.3 <sup>f</sup>
C <sub>2</sub> H <sub>2</sub>	1 $\pi_u$ (HOMO)	11.2		11.4 <sup>e</sup>
	3 $\sigma_g$ (HOMO-1)	15.7		16.4 <sup>e</sup>

<sup>a</sup>Reference [28]

<sup>b</sup>Reference [42]

<sup>c</sup>Reference [43]

<sup>d</sup>Reference [6]

<sup>e</sup>Reference [44]

<sup>f</sup>Reference [45]

be readily calculated.

In Fig. 3, we compare the ionization rates from N<sub>2</sub>, O<sub>2</sub> and CO<sub>2</sub> molecules, for the HOMO, HOMO-1 and HOMO-2 orbitals, at peak intensities indicated in the figure. Note that the angular dependence,  $P(\theta)$ , reflects the symmetry of the molecular orbital quite accurately. Thus a  $\sigma$  orbital tends to have the peak at 0° and a minimum at 90°, a  $\pi_g$  orbital has the peak near 45° and minimum at 0° and 90°, and a  $\pi_u$  orbital has a peak near 90° and minimum near 0° (Deviations do occur, see the HOMO-1 of CO<sub>2</sub> in Fig. 3(c)). These general behaviors of ionization rates explain why HOMO-2 is bigger than HOMO-1 at small angles for N<sub>2</sub>, O<sub>2</sub>, and CO<sub>2</sub>, and why HOMO-1 is more important than HOMO at small angles for C<sub>2</sub>H<sub>2</sub>. Note that the relative ionization rates depend on laser intensities. The relative ionization rates for inner orbitals increases faster with increasing laser intensities. Using the parameters in Table V, their relative rates can be easily calculated using the MO-ADK model. We have also calculated the ionization rates using the molecular SFA. The relative alignment dependence from SFA in general agrees with those shown in Fig. 3. This is consistent with the findings in Le *et al.* [35].

Fig. 4 shows the HOMO and HOMO-1 ionization rates for asymmetric diatomic molecules CO and HCl. There are recent experiments and other theoretical calculations

TABLE V: The  $C_l$  coefficients of HOMO, HOMO-1 and HOMO-2 for N<sub>2</sub>, O<sub>2</sub> and CO<sub>2</sub> and of HOMO, HOMO-1 for CO, HCl and C<sub>2</sub>H<sub>2</sub>. For  $\sigma$  orbital, m=0 and  $\pi$  orbital, m=1.

Molecule	Spin orbital	$C_l$			
N <sub>2</sub>	3 $\sigma_g$ (HOMO)	$C_{0m}$	$C_{2m}$	$C_{4m}$	
		2.68	1.10	0.06	
		$C_{1m}$	$C_{3m}$	$C_{5m}$	
	1 $\pi_u$ (HOMO-1)	1.89	0.22	0.01	
O <sub>2</sub>	2 $\sigma_u$ (HOMO-2)	3.72	0.34	0.01	
			$C_{2m}$	$C_{4m}$	
			0.52	0.03	
	1 $\pi_g$ (HOMO)		$C_{1m}$	$C_{3m}$	$C_{5m}$
CO <sub>2</sub>	1 $\pi_u$ (HOMO-1)	2.04	0.33	0.01	
			$C_{0m}$	$C_{2m}$	$C_{4m}$
			3.05	1.59	0.08
	3 $\sigma_g$ (HOMO-2)		$C_{2m}$	$C_{4m}$	$C_{6m}$
CO	1 $\pi_g$ (HOMO)	1.97	0.40	0.04	
			$C_{1m}$	$C_{3m}$	$C_{5m}$
			3.33	1.31	0.18
	1 $\pi_u$ (HOMO-1)		$C_{0m}$	$C_{1m}$	$C_{2m}$
HCl	3 $\sigma_u$ (HOMO-2)	7.50	2.58	0.32	0.03
			$C_{0m}$	$C_{1m}$	$C_{2m}$
			2.32	1.62	0.82
	5 $\sigma$ (HOMO)		$C_{1m}$	$C_{2m}$	$C_{3m}$
C <sub>2</sub> H <sub>2</sub>	1 $\pi$ (HOMO-1)	1.73	0.14	0.21	0.02
			$C_{0m}$	$C_{1m}$	$C_{2m}$
			1.23	0.01	0.05
	2 $\pi$ (HOMO)		$C_{0m}$	$C_{1m}$	$C_{2m}$
CO	5 $\sigma$ (HOMO-1)	0.10	2.64	0.57	0.25
			$C_{0m}$	$C_{1m}$	$C_{2m}$
			0.10	2.64	0.57
	1 $\pi_u$ (HOMO)		$C_{1m}$	$C_{3m}$	$C_{5m}$
HCl	1 $\pi_u$ (HOMO)	1.16	0.18	0.02	
			$C_{0m}$	$C_{2m}$	$C_{4m}$
			4.40	3.85	0.72
	3 $\sigma_g$ (HOMO-1)		$C_{0m}$	$C_{2m}$	$C_{4m}$

available for these two molecules [5, 36]. For both systems, the predictions from MO-ADK are also compared to results from SFA. Refer to Table IV, we note that the difference in binding energies between HOMO and HOMO-1 in CO is 2.9 eV, and 3.5 eV for HCl. First we examine the  $\theta$ -dependence predicted by MO-ADK in Figs. 4(a) and 4(b). The HOMO of CO is a  $\sigma$  orbital, its  $P(\theta)$  drops rapidly from 0° to 90° and stays relative flat at larger angles. The HOMO-1 is a  $\pi$  orbital and its  $P(\theta)$  peaks near 90°. For HCl, the HOMO is a  $\pi$  orbital and it peaks near 90°. For the HOMO-1, it is a  $\sigma$  orbital and its  $P(\theta)$  drops steadily till near 90°. Interestingly, its  $P(\theta)$  increases rapidly from 90° to 180°, making it almost like a symmetric molecule.

Why are the  $\sigma$  orbitals of the two molecules so different? It is due to the degree of asymmetry in the wavefunctions. Such asymmetry is reflected in the  $C_l$  coefficients in Table V. For CO (HCl), the first three coefficients are 2.32, 1.62, 0.82 (0.10, 2.64, 0.57) for  $l=0, 1$  and

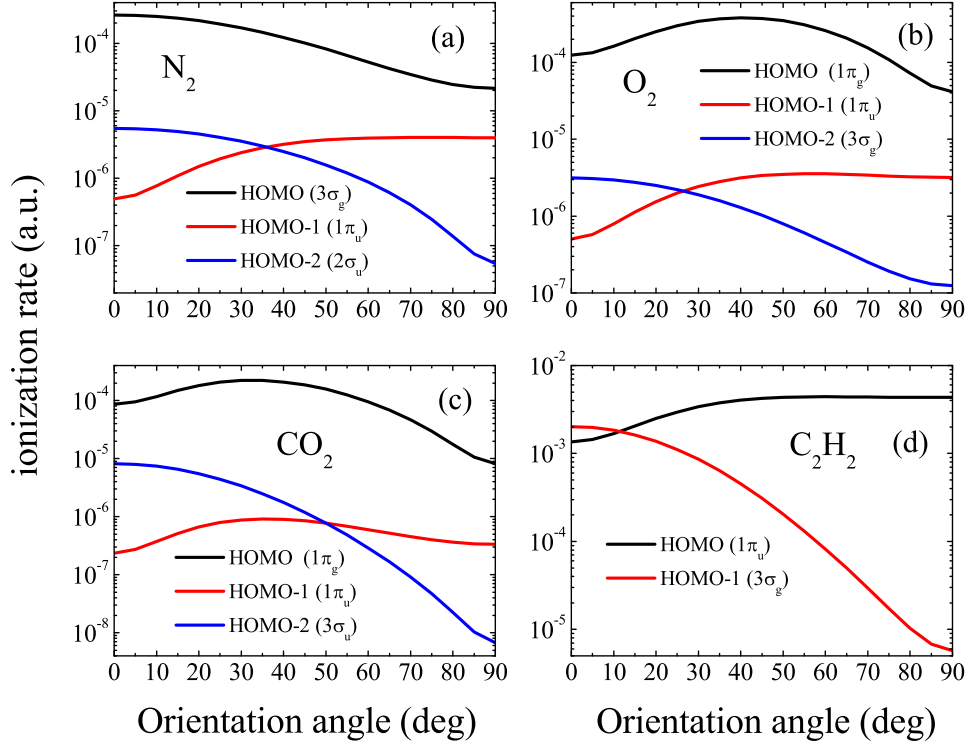


FIG. 3: (Color online) Alignment dependence of ionization rates of HOMO, HOMO-1 and HOMO-2 for  $\text{N}_2$ ,  $\text{O}_2$  and  $\text{CO}_2$  and of HOMO and HOMO-1 for  $\text{C}_2\text{H}_2$ . (a)  $\text{N}_2$  at laser intensity of  $1.5 \times 10^{14} \text{ W/cm}^2$ ; (b)  $\text{O}_2$  at  $1.3 \times 10^{14} \text{ W/cm}^2$ ; (c)  $\text{CO}_2$  at  $1.1 \times 10^{14} \text{ W/cm}^2$ ; (d)  $\text{C}_2\text{H}_2$  at  $1.5 \times 10^{14} \text{ W/cm}^2$ .

2, respectively. For  $\text{HCl}$ , there is one dominant  $l=1$  component only, thus the ionization rate is nearly symmetric. For  $\text{CO}$ , the two coefficients for  $l=0$  and 1 are comparable, the wavefunction along the axis for  $\theta = 0$  and  $\theta = \pi$  has the ratio  $(2.32+1.62)/(2.32-1.62)=5.6$ . This gives a ionization rate ratio of 32, close to the value 50 read off from Fig. 4(a).

In Figs. 4(a) and 4(b), the  $\theta$ -dependence from SFA is different from MO-ADK. Recall that in MO-ADK, static ionization rate was calculated, thus a molecule is AB or BA with respect to the fixed electric field will have different rates. For a linearly polarized laser pulse, the direction of the electric field changes after each half cycle, thus the cycle-averaged rates for AB and BA are identical. To compare the SFA rate with the MO-ADK rate at an angle  $\theta$ , we have to average the rates from the latter at  $\theta$  and  $\pi-\theta$ . These “symmetrized” ionization rates are denoted by MO-ADK-S in Fig. 4. By comparing the rates from SFA and MO-ADK-S, we found in Fig. 4(c) that the two models agree well for  $\text{CO}$ . For  $\text{HCl}$ , the relative rates for HOMO-1, normalized to HOMO, are about a factor of two larger from SFA than from MO-ADK. We comment that if ionization is measured using circularly polarized light, the static MO-ADK rate can be compared directly

with the rate calculated using SFA.

The results of Figs. 3 and 4 show that at alignment angles where tunneling ionization from the HOMO is large, contributions from HOMO-1 or other inner orbitals are negligible. At alignment angles where HOMO is near the minimum, if the HOMO-1 (or even HOMO-2) is near the maximum, then these inner orbitals may become important. Since the relative tunneling ionization rates also depend on the peak laser intensity, when multiple orbitals contribute to strong field phenomena, the intensity dependence may become prominent. Experimentally, such multiple orbital effects have been observed in HHG from  $\text{N}_2$  when molecules are aligned perpendicular to the laser’s polarization axis [34, 35]. The inner orbitals have been shown to become important in HHG from  $\text{CO}_2$  when the molecules are aligned parallel to the laser’s polarization axis [37]. Comparing to single photon ionization, strong field ionization tends to be more selective by ionizing the HOMO. For single photon ionization, cross sections for HOMO, HOMO-1 and HOMO-2 in general have comparable values and often cross sections from inner orbitals are higher, see e.g., [46] for  $\text{CO}_2$ .

There are few theoretical alignment-dependent ionization rates from inner orbitals available to compare with

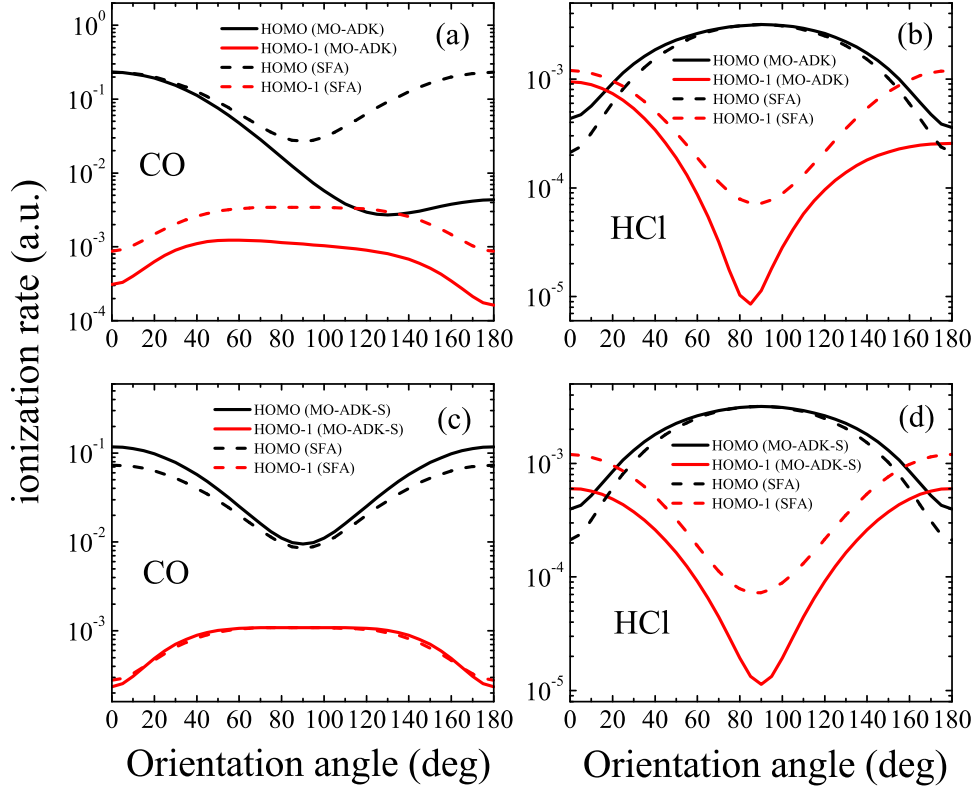


FIG. 4: (Color online) Alignment dependence of ionization rates of HOMO and HOMO-1. (a) CO at laser intensity of  $4 \times 10^{14}$  W/cm<sup>2</sup>; (b) HCl at  $2 \times 10^{14}$  W/cm<sup>2</sup>; (c) CO at  $4 \times 10^{14}$  W/cm<sup>2</sup>; (d) HCl at  $2 \times 10^{14}$  W/cm<sup>2</sup>. MO-ADK-S is the averaged MO-ADK rate for angles  $\theta$  and  $\pi - \theta$ .

the predictions of the MO-ADK theory presented here. There is an exception, however, CO<sub>2</sub>. In [47] ionization rates from HOMO, HOMO-1 and HOMO-2 have been calculated starting from the multielectron perspective. In Fig. 5(a) we compare the rates from MO-ADK with those from [47] at the uncoupled channel approximation. The two sets of calculations are normalized at the peak of the HOMO curve. We note that the  $\theta$ -dependence agrees well for each orbital. For the HOMO, the agreement is “perfect”. The rates for the inner orbitals are larger from [47] than from MO-ADK. Part of the reason of the larger difference in the HOMO-1 rate could be due to the difference in the ionization energy used. In [47], the energy difference between HOMO-1 and HOMO was taken to be 3.53 eV, while in MO-ADK, the difference was taken to be 3.80 eV from the experimental values in Table IV. For the HOMO-2 the energy used is the same for the two calculations. The alignment dependence of ionization rates for the three orbitals have also been calculated in [37] and the comparison with the present MO-ADK is given in Fig. 5(b), again by normalizing at the peak value of the HOMO. In this case the differences are

larger. In [37], the ionization rates were calculated using Coulomb corrected SFA plus sub-cycle dynamics. The TDDFT method has also been used to obtain ionization probabilities from different orbitals [6, 28]. For CO<sub>2</sub>, the predicted alignment dependence for the HOMO, HOMO-1 and HOMO-2 as shown in Fig. 3 of [6] do agree with the present Fig. 3(c), including that the peak for HOMO-1 is not at 90°. However, we should comment that in N<sub>2</sub> and O<sub>2</sub>, the alignment dependence using the same TDDFT method in [28] does not agree with Figs. 3(a) and 3(b) shown for these two molecules.

### E. Comparisons with Experiments

Fig. 6 shows the normalized alignment dependence of ionization probability of N<sub>2</sub>, O<sub>2</sub>, H<sub>2</sub> and HCl. From Figs. 6(a) and 6(b), we comment that the normalized ionization probability of N<sub>2</sub> calculated from MO-ADK theory using the old and the newly fitted coefficients agree quite well (no visible difference in the plot). Compared to the experiment of Pavičić *et al.* [3], the MO-ADK theory

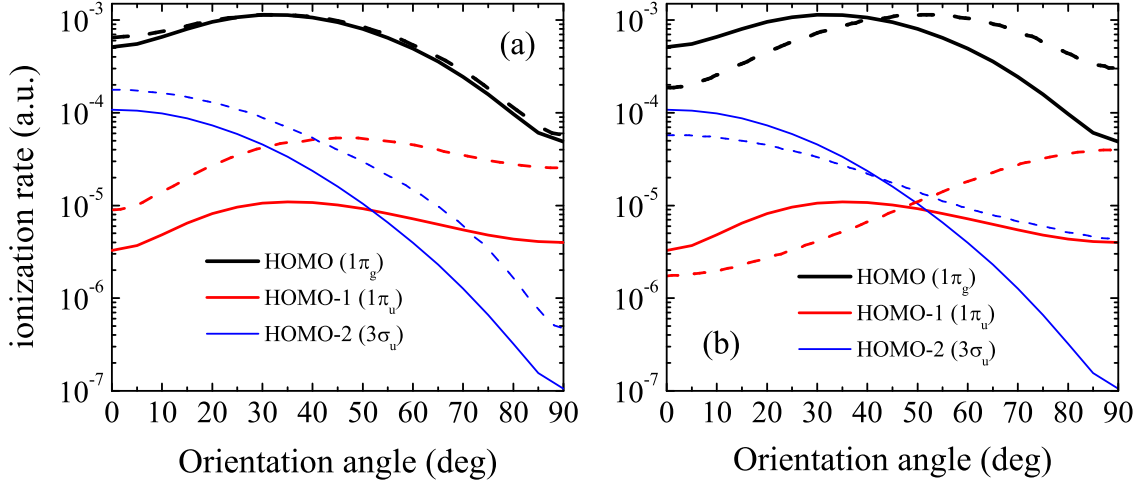


FIG. 5: (Color online) Comparison of ionization rates of HOMO, HOMO-1 and HOMO-2 of  $\text{CO}_2$  at peak laser intensity of  $1.5 \times 10^{14} \text{ W/cm}^2$ . The solid lines are from MO-ADK and the dashed lines are from Spanner and Patchkovskii [47] (a) and from Smirnova *et al.* [37] (b).

shows some differences. But the difference is considered acceptable. Note that the determination of alignment dependence from the experiment has angular average which was not included in the theory curve. Take the experimental result as reference, the TDDFT result (see Fig. 2) is better than the MO-ADK for  $\text{N}_2$ . For  $\text{O}_2$ , it is the other way around. The same comparison for  $\text{CO}_2$  has been addressed in an earlier paper [19]. In that case, the old MO-ADK results were found to be inaccurate due to the inaccuracy of the old  $C_l$  parameters. In [19] it was further concluded that the experimental  $P(\theta)$  from [3] appears to be too narrowly peaked. We note that the new result from [47] also does not agree with the experiment. However the authors suspect that the discrepancy is due to intermediate excitation channels were not included in their calculation. We tend to think that additional experiments are needed to help resolving this discrepancy.

In Fig. 2(e) we show that the MO-ADK probabilities for  $\text{H}_2$  using the new structure parameters are different from using the earlier ones [9]. The new MO-ADK probabilities and molecular SFA agree well, see Fig. 6(c). Comparing to experimental data of Staudte *et al.* [4], the agreement is good in view that the theory curve has not included average over angular resolution. In [4], the ratio of ionization rate for molecules aligned parallel vs perpendicular, with respect to the polarization axis, were also determined at four intensities from 2 to  $4.5 \times 10^{14} \text{ W/cm}^2$  (for circularly polarized laser). The ratio from the present SFA (not shown) agree with the SFA model in that paper, and with the new MO-ADK ratio of 1.45 (the old MO-ADK gives 1.15). We expect the theoretical

ratio be reduced somewhat if angular average is incorporated. We mention that a similar measurement at one intensity for laser wavelength of 1850 nm was reported in [48], which gives a ratio of 1.15. Interestingly, this ratio was reported to be 3.0 [49] in another recent experiment, while the theory presented in the same paper gives a ratio of 2.1. We comment that the ratio is taken at the maximum with respect to the minimum and thus sensitive to the angular average. Comparison of the rates over the whole angular range would be preferable.

In Fig. 6(d), the  $P(\theta)$  of the HOMO-1 orbital in HCl reported in Ref. [5] using circularly polarized light at the intensity of  $1.4 \times 10^{14} \text{ W/cm}^2$  is shown. We compare the HOMO-1 result from the MO-ADK theory using the laser parameters given in the experiment, and by normalizing the data at  $\theta=0^\circ$ . In Ref. [5], the alignment dependence for HOMO and HOMO-1 has also been reported using the TDDFT. The alignment dependence between MO-ADK and TDDFT calculations are quite similar, but our relative HOMO-1 probability is about a factor of three higher at the same laser intensity. The ionization probability from both calculations drop much faster from  $0^\circ$  to  $90^\circ$  when compared to the experiment. By introducing a small fraction of the contribution from the HOMO in the manner suggested in [5], the MO-ADK theory can achieve a reasonable agreement with the experimental data from  $0^\circ$  to  $90^\circ$ , see Fig. 6(d). On the other hand, the agreement at angles larger than  $90^\circ$  is still not as good.

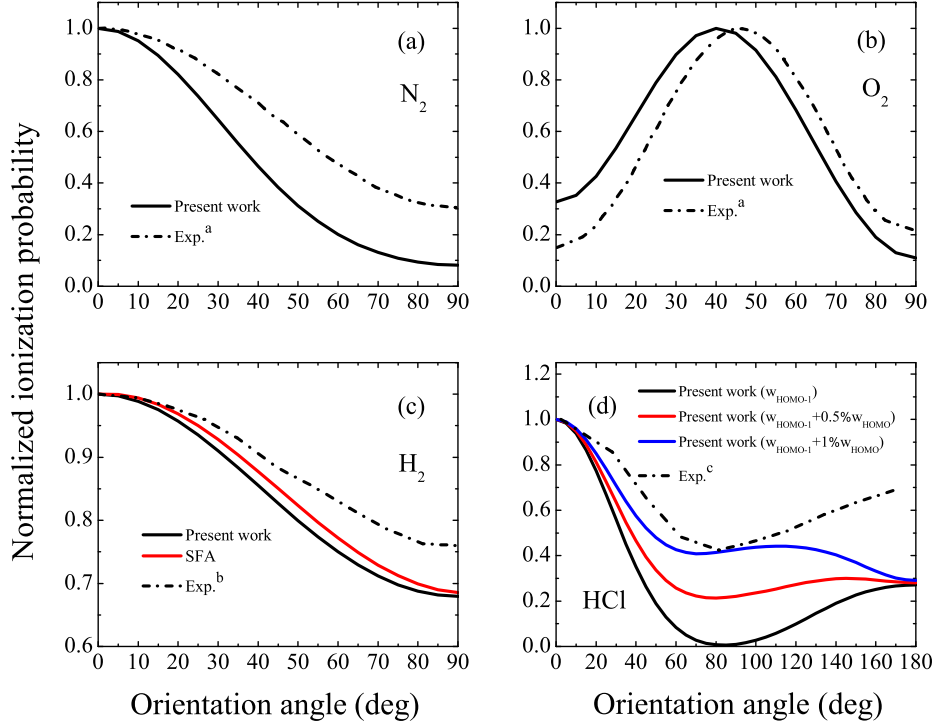


FIG. 6: (Color online) Normalized alignment dependence of ionization probability. (a)  $\text{N}_2$  at laser intensity of  $1.5 \times 10^{14}$  W/cm $^2$ ; (b)  $\text{O}_2$  at  $1.3 \times 10^{14}$  W/cm $^2$ ; (c)  $\text{H}_2$  at  $2.3 \times 10^{14}$  W/cm $^2$ ; (d)  $\text{HCl}$  at  $1.4 \times 10^{14}$  W/cm $^2$ . Linearly polarized lights for (a) and (b); Circularly polarized lights for (c) and (d). Exp.<sup>a</sup> from Pavičić *et al.* [3]; Exp.<sup>b</sup> from Staudte *et al.* [4] and Exp.<sup>c</sup> from Akagi *et al.* [5]. Additional symbols for (d), see text.

### F. Ionization probability of $\text{H}_2^+$

The ionization probability of  $\text{H}_2^+$  has been calculated from solving the TDSE by different groups [32, 33, 50]. It is of interest to compare the predictions based on MO-ADK with those from solving the TDSE. In Fig. 7, the normalized alignment-dependent ionization probability from the first four molecular orbitals of  $\text{H}_2^+$  at the equilibrium distance are shown. The data for  $1s\sigma_g$  have been discussed earlier [19]. For ionization from  $1s\sigma_u$ , the two TDSE calculations and the MO-ADK agree quite well. For  $2p\pi_u$ , the MO-ADK theory tends to peak at  $90^\circ$  while the TDSE result gives a peak closer to about  $60^\circ$ . For  $2p\pi_g$  state, the MO-ADK predicts a peak near  $45^\circ$  while TDSE calculation gives a peak at about  $55^\circ$ . Note different peak laser intensities are used for the ionization from each orbital.

In Fig. 8(a) we show the dependence of normalized ionization probabilities vs the internuclear separation for the  $1s\sigma_{g,u}$  states of  $\text{H}_2^+$  with the molecular axis parallel to the polarization axis. The results are compared to the TDSE calculations of [51]. By normalizing the probability at  $R = 2$  a.u. for the  $1s\sigma_u$ , we find that there is

a general good agreement between the TDSE result and from the MO-ADK. For the  $1s\sigma_g$ , the two calculations are normalized at  $R = 4.0$  a.u.. For both calculations, the probabilities at  $R$  less than  $3.5$  a.u. are significantly smaller than at  $R = 4.0$  a.u.. In Figs. 8(b) and 8(c), the normalized alignment-dependent ionization rates are shown for different  $R$ . Clearly as  $R$  increases, the angular dependence becomes sharper. This is easily understood for  $\sigma$  orbitals since the molecular orbital becomes more elongated along the molecular axis as  $R$  increases. The  $C_l$  coefficients are tabulated in Table VI to reflect how these parameters vary as  $R$  increases.

## IV. CONCLUSIONS

In this paper we proposed a new method to obtain accurate molecular wavefunctions in the asymptotic region starting with molecular orbitals obtained from the widely used quantum chemistry packages such as GAMESS and GAUSSIAN. From these wavefunctions, the structure parameters in the molecular tunneling ionization theory (MO-ADK) of Tong *et al.* [9] can be

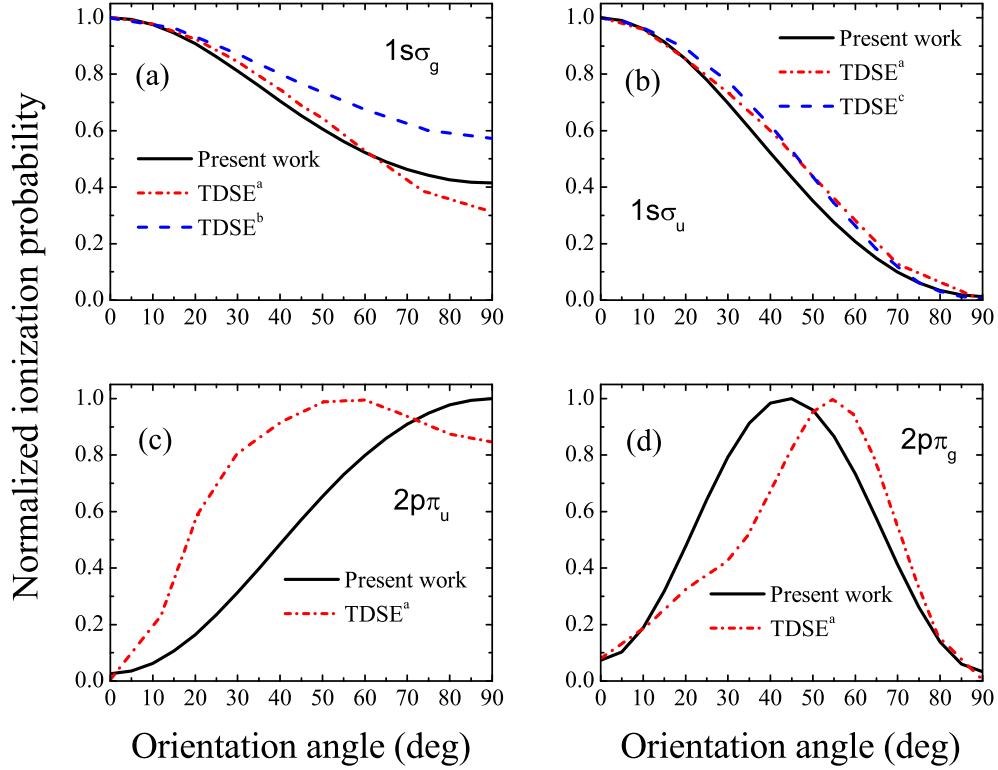


FIG. 7: (Color online) Normalized alignment dependence of ionization probability of  $H_2^+$ . (a)  $1s\sigma_g$  at laser intensity of  $5 \times 10^{14}$  W/cm<sup>2</sup>; (b)  $1s\sigma_u$  at  $10^{14}$  W/cm<sup>2</sup>; (c)  $2p\pi_u$  at  $10^{13}$  W/cm<sup>2</sup>; (d)  $2p\pi_g$  at  $10^{12}$  W/cm<sup>2</sup>. TDSE<sup>a</sup> from Kamta *et al.* [32], TDSE<sup>b</sup> from Kjeldsen *et al.* [33] and TDSE<sup>c</sup> from Telnov *et al.* [50].

accurately determined. Using these structure parameters, we re-examined the alignment-dependent tunneling ionization probabilities for a number of molecules, including ionization from HOMO-1 and HOMO-2 orbitals. The calculated tunneling ionization probabilities are compared to probabilities determined from experiments, and to several other more elaborated calculations. Since tunneling ionization is the first step for strong field phenomena involving molecular targets, these structure parameters are useful and thus are tabulated. The procedure for obtaining the structure parameters discussed in this paper is generally applicable to any linear molecules. Despite of its fundamental importance, accurate strong field alignment-dependent ionization probabilities are still not widely available. Experimental measurements as well as more advanced calculations tend to deal with different molecules and under different

conditions, thus it is difficult to benchmark the accuracy of the theoretical models. While MO-ADK model is the simplest model for obtaining tunneling ionization rates, it appears that its predictions so far are in good agreement with most of the experimental data and with most the elaborate theoretical calculations.

### Acknowledgments

This work was supported in part by Chemical Sciences, Geosciences and Biosciences Division, Office of Basic Energy Sciences, Office of Science, U.S. Department of Energy. S.-F.Z was also supported by the National Natural Science Foundation of China under Grant No.10674112.

- 
- [1] A. S. Alnaser *et al.*, Phys. Rev. Lett. **93**, 113003 (2004).
  - [2] I. V. Litvinyuk, K. F. Lee, P. W. Dooley, D. M. Rayner,

D. M. Villeneuve, and P. B. Corkum, Phys. Rev. Lett. **90**, 233003 (2003).

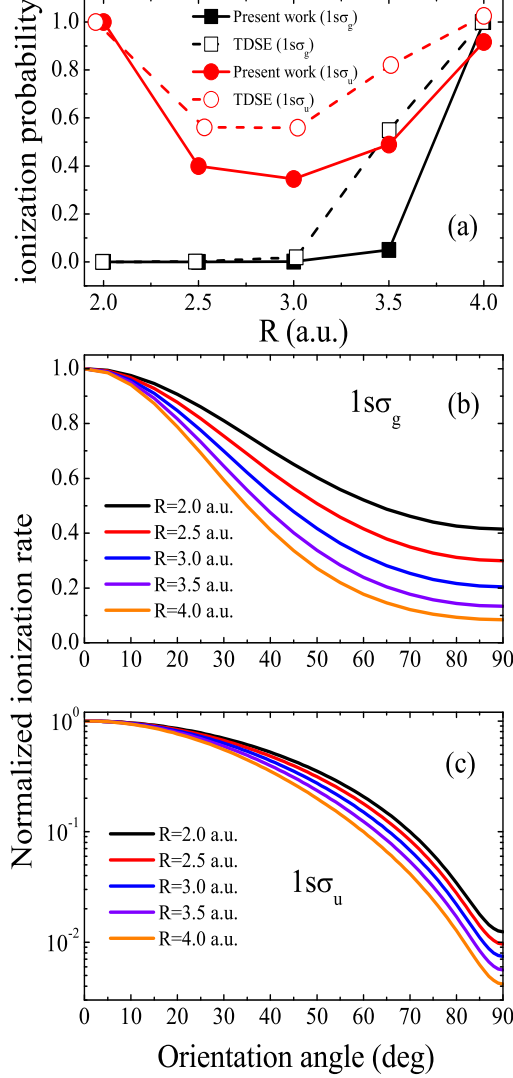


FIG. 8: (Color online) (a) R-dependence of the normalized ionization probability of  $H_2^+$  at laser intensity of  $10^{14}$  W/cm<sup>2</sup>; see text. (b) The normalized alignment dependence of ionization rate at  $5 \times 10^{14}$  W/cm<sup>2</sup> for  $1s\sigma_g$ ; (c) The normalized alignment dependence of ionization rate at  $10^{14}$  W/cm<sup>2</sup> for  $1s\sigma_u$ . TDSE from [51].

[3] D. Pavičić, K. F. Lee, D. M. Rayner, P. B. Corkum, and D. M. Villeneuve, Phys. Rev. Lett. **98**, 243001 (2007).  
 [4] A. Staudte, S. Patchkovskii, D. Pavičić, H. Akagi, O. Smirnova, D. Zeidler, M. Meckel, D. M. Villeneuve, R. Dörner, M. Yu. Ivanov, and P. B. Corkum, Phys. Rev. Lett. **102**, 033004 (2009).  
 [5] H. Akagi, T. Otobe, A. Staudte, A. Shiner, F. Turner, R. Dörner, D. M. Villeneuve, and P. B. Corkum, Science **325**, 1364 (2009).  
 [6] S. K. Son and Shih-I Chu, Phys. Rev. A **80**, 011403(R) (2009).  
 [7] J. Muth-Böhm, A. Becker, and F. H. M. Faisal, Phys.

TABLE VI: The  $C_l$  coefficients of  $1s\sigma_g$ ,  $1s\sigma_u$ ,  $2p\pi_g$  and  $2p\pi_u$  for  $H_2^+$  at different internuclear distances. For  $\sigma$  orbital,  $m=0$  and  $\pi$  orbital,  $m=1$ . The calculated binding energies and exact ones (in atomic units) are also listed.

symmetry	$R$ (a.u.)	binding energy		$C_l$		
$1s\sigma_g$		Present	Exact	$C_{0m}$	$C_{2m}$	$C_{4m}$
	2.0	1.1025	1.1026	4.52	0.62	0.03
	2.5	0.9937	0.9938	4.25	0.81	0.05
	3.0	0.9107	0.9109	4.10	1.04	0.08
	3.5	0.8463	0.8466	4.00	1.31	0.12
$1s\sigma_u$	4.0	0.7958	0.7961	3.96	1.60	0.19
				$C_{1m}$	$C_{3m}$	$C_{5m}$
	2.0	0.6674	0.6675	1.89	0.08	0.00
	2.5	0.6920	0.6921	2.18	0.15	0.00
	3.0	0.7012	0.7014	2.48	0.25	0.01
$2p\pi_g$	3.5	0.7009	0.7012	2.79	0.37	0.02
	4.0	0.6952	0.6956	3.13	0.53	0.04
				$C_{2m}$	$C_{4m}$	
	2.0	0.4288	0.4288	0.11	0.002	
$2p\pi_u$				$C_{1m}$	$C_{3m}$	
	2.0	0.2267	0.2267	0.90	0.02	

Rev. Lett. **85**, 2280 (2000).  
 [8] T. K. Kjeldsen and L. B. Madsen, J. Phys. B **37**, 2033 (2004).  
 [9] X. M. Tong, Z. X. Zhao, and C. D. Lin, Phys. Rev. A **66**, 033402 (2002).  
 [10] M. V. Ammosov, N. B. Delone, and V. P. Krainov, Zh. Eksp. Teor. Fiz. **91**, 2008 (1986) [Sov. Phys. JETP **64**, 1191 (1986)].  
 [11] Z. X. Zhao and T. Brabec, J. Phys. B **39**, L345 (2006).  
 [12] T. Brabec, M. Côté, P. Boulanger, and L. Ramunno, Phys. Rev. Lett. **95**, 073001 (2005).  
 [13] I. I. Fabrikant and G. A. Gallup, Phys. Rev. A **79**, 013406 (2009).  
 [14] D. Dill and J. L. Dehmer, J. Chem. Phys. **61**, 692 (1974).  
 [15] M. W. Schmidt *et al.*, J. Comput. Chem. **14**, 1347 (1993).  
 [16] M. J. Frisch *et al.*, GAUSSIAN 03, Revision C.02 (Gaussian Inc. Pittsburgh, PA, 2003).  
 [17] A. -T. Le, X. M. Tong, and C. D. Lin, J. Mod. Opt. **54**, 967 (2007).  
 [18] T. K. Kjeldsen and L. B. Madsen, Phys. Rev. A **71**, 023411 (2005).  
 [19] S. -F. Zhao, C. Jin, A. -T. Le, T. F. Jiang, and C. D. Lin, Phys. Rev. A **80**, 051402(R) (2009).  
 [20] X. M. Tong and C. D. Lin, J. Phys. B **38**, 2593 (2005).  
 [21] M. Abu-samha and L. B. Madsen, Phys. Rev. A **80**, 023401 (2009).  
 [22] R. van Leeuwen and E. J. Baerends, Phys. Rev. A **49**, 2421 (1994).  
 [23] P. R. T. Schipper, O. V. Gritsenko, S. J. A. van Gisbergen, and E. J. Baerends, J. Chem. Phys. **112**, 1344 (2000).  
 [24] Shih-I Chu, J. Chem. Phys. **123**, 062207 (2005).  
 [25] H. Bachau, E. Cormier, P. Decleva, J. E. Hansen, and F. Martín, Rep. Prog. Phys. **64**, 1815 (2001).  
 [26] A. Banerjee and M. K. Harbola, Phys. Rev. A **60**, 3599

- (1999).
- [27] J. Emsley, *The Elements* (Clarendon Press, Oxford, 1998).
  - [28] D. A. Telnov and Shih-I Chu, Phys. Rev. A **79**, 041401(R) (2009).
  - [29] M. Awasthi, Y. V. Vanne, A. Saenz, A. Castro, and P. Decleva, Phys. Rev. A **77**, 063403 (2008).
  - [30] C. D. Lin, X. M. Tong, and Z. X. Zhao, J. Mod. Opt. **53**, 21 (2006).
  - [31] T. Otake and K. Yabana, Phys. Rev. A **75**, 062507 (2007).
  - [32] G. L. Kamta and A. D. Bandrauk, Phys. Rev. A **74**, 033415 (2006).
  - [33] T. K. Kjeldsen, L. A. A. Nikolopoulos, and L. B. Madsen, Phys. Rev. A **75**, 063427 (2007).
  - [34] B. K. McFarland, J. P. Farrell, P. H. Bucksbaum, and M. Gühr, Science **322**, 1232 (2008).
  - [35] A. -T. Le, R. R. Lucchese, and C. D. Lin, J. Phys. B **42**, 211001 (2009).
  - [36] I. Znakovskaya, P. von den Hoff, S. Zherebtsov, A. Wirth, O. Herrwerth, M. J. J. Vrakking, R. de Vivie-Riedle, and M. F. Kling, Phys. Rev. Lett. **103**, 103002 (2009).
  - [37] O. Smirnova *et al.*, Nature (London) **460**, 972 (2009).
  - [38] T. Morishita, A. -T. Le, Z. Chen, and C. D. Lin, Phys. Rev. Lett. **100**, 013903(2008).
  - [39] Z. Chen, A. -T. Le, T. Morishita, and C. D. Lin, Phys. Rev. A **79**, 033409 (2009).
  - [40] A. -T. Le, R. R. Lucchese, S. Tonzani, T. Morishita, and C. D. Lin, Phys. Rev. A **80**, 013401 (2009).
  - [41] S. Micheau, Z. Chen, A. -T. Le, and C. D. Lin, Phys. Rev. A **79**, 013417 (2009).
  - [42] A. Lofthus and P. H. Krupenie, J. Phys. Chem. Ref. Data **6**, 113 (1977).
  - [43] P. Baltzer, B. Wannberg, L. Karlsson, M. Carlsson Göthe, and M. Larsson. Phys. Rev. A **45**, 4374 (1992).
  - [44] D. W. Turner *et al.*, *Molecular Photoelectron Spectroscopy* (Wiley-Interscience, London, 1970).
  - [45] P. Natalis, P. Pernetreau, L. Longton, and J. E. Collin, J. Electron Spectrosc. Relat. Phenom. **27**, 267 (1982).
  - [46] R. R. Lucchese and V. McKoy, Phys. Rev. A **26**, 1406 (1982).
  - [47] M. Spanner and S. Patchkovskii, Phys. Rev. A **80**, 063411 (2009).
  - [48] M. Magrakvelidze, F. He, S. De, I. Bocharova, D. Ray, U. Thumm, and I. V. Litvinyuk, Phys. Rev. A **79**, 033408 (2009).
  - [49] P. von den Hoff, I. Znakovskaya, S. Zherebtsov, M. F. Kling, and R. de Vivie-Riedle, Appl. Phys. B: Lasers Opt. (online available).
  - [50] D. A. Telnov and Shih-I Chu, Phys. Rev. A **76**, 043412 (2007).
  - [51] G. L. Kamta and A. D. Bandrauk, Phys. Rev. A **75**, 041401(R) (2007).